PHYSOR 2012 – Advances in Reactor Physics – Linking Research, Industry, and Education
Knoxville, Tennessee, USA, April 15-20, 2012, on CD-ROM, American Nuclear Society, LaGrange Park, IL (2012)

SCALE CODE VALIDATION FOR PRISMATIC HIGH-TEMPERATURE GAS-COOLED REACTORS[1]

Dan Ilas
Oak Ridge National Laboratory
P.O. Box 2008, Oak Ridge, TN 37831-6170, USA
ilasd@ornl.gov

ABSTRACT

Using experimental data published in the *International Handbook of Evaluated Reactor Physics Benchmark Experiments* for the fresh cold core of the High Temperature Engineering Test Reactor, a comprehensive validation study has been carried out to assess the performance of the SCALE code system for analysis of high-temperature gas-cooled reactor configurations. This paper describes part of the results of that effort. The studies performed included criticality evaluations for the full core and for the annular cores realized during the fuel loading, as well as calculations and comparisons for excess reactivity, shutdown margin, control rod worths, temperature coefficient of reactivity, and reaction rate distributions. Comparisons of the SCALE results with both experimental values and MCNP-calculated values are presented. The comparisons show that the SCALE calculated results, obtained with both multigroup and continuous energy cross sections, are in reasonable agreement with the experimental data and the MCNP predictions.

Key Words: HTGR, HTTR, SCALE, code validation.

1. INTRODUCTION

The SCALE code system [1] developed at Oak Ridge National Laboratory (ORNL) has been used for many years for various light water reactor applications. In recent years, features that allow handling of problems specific to high-temperature gas-cooled reactors (HTGRs) have been added. Such specific features include the treatment of the double-heterogeneity of the fuel that is characteristic of HTGRs, for both the prismatic (cylindrical fuel pins) and pebble bed designs.

The present study focuses on the validation of SCALE for prismatic designs by modeling the cold core experiments performed at the Japanese High Temperature Engineering Test Reactor (HTTR) as described in the *International Handbook of Evaluated Reactor Physics Benchmark Experiments* (IRPhE) ([2], [3], [4]). The study uses the latest revisions of the IRPhE benchmark descriptions. A previous comprehensive validation study [5] was undertaken at ORNL that used earlier versions of these benchmarks. The SCALE models developed for various HTTR configurations were used to assess different parameters of importance to the operation of this reactor and to compare the calculated results with experimental data.

[1] This manuscript has been authored by UT-Battelle, LLC, under contract DE-AC05-00OR22725 with the U.S. Department of Energy. The United States Government retains and the publisher, by accepting the article for publication, acknowledges that the United States Government retains a non-exclusive, paid-up, irrevocable, world-wide license to publish or reproduce the published form of this manuscript, or allow others to do so, for United States Government purposes.

Section 2 of this paper presents a brief description of HTTR. The codes and nuclear data used to develop the SCALE models are summarized in Section 3. The results of the simulations are presented and discussed in Section 4.

2. DESCRIPTION OF HTTR CONFIGURATIONS

HTTR is a 30 MWth, prismatic core, graphite-moderated, helium-cooled reactor built by the Japan Atomic Energy Agency. The core of this reactor consists of fuel blocks that use tristructural-isotropic (TRISO) fuel with 12 different fuel enrichments, between 3.4 wt% and 9.9 wt% ^{235}U/U, grouped into four fuel zones across the core. The fuel blocks are arranged in five-block columns, for a total active height of 290 cm, which in turn make up four fuel zones that are intermixed with control rod columns and surrounded by reflector blocks. Figure 1 shows a cross sectional view of the HTTR fully loaded (30 fuel columns) core as modeled with SCALE.

The control rods, made of B_4C, are operated in pairs. Each pair of control rods occupies two of the three available channels in each control rod guide column. There are a total of 16 pairs of control rods in the HTTR core. The third hollow position in each control rod guide column can be used as a reserved shutdown pellet insertion hole. These pellets, also made of B_4C, can be released into the holes under gravity as a backup mechanism for emergency shutdown. In addition to the fuel and control blocks, the active core contains three columns reserved for irradiation tests and 12 replaceable reflector columns.

The IG-110 graphite used in the fabrication of the fuel blocks, control rod blocks, irradiation blocks and replaceable reflector blocks is a high-purity graphite with an equivalent boron content (EBC) below 1 ppm. The EBC of the PGX graphite used for the permanent reflector is below 5 ppm. During the approach to criticality, dummy graphite blocks are also used to replace the fuel blocks. These blocks are fabricated from IG-11 graphite, which also has an EBC below 5 ppm.

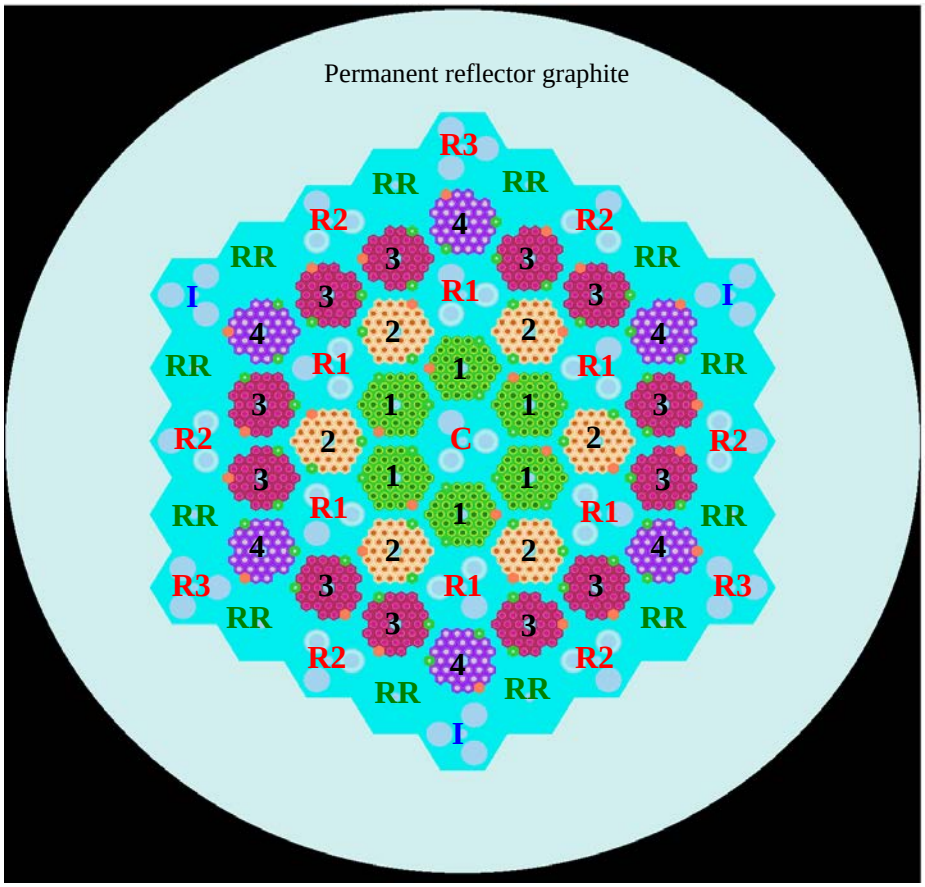

Fuel zones: **1**, **2**, **3**, **4**
Control rods: **C** central
R1 ring 1
R2 ring 2
R3 ring 3
I Instrumentation column
RR Replaceable reflector column

Figure 1. Fully loaded HTTR core configuration (SCALE model).

2.1. Fuel Blocks

The HTTR fuel blocks are hexagonal prisms that can contain either 31 or 33 fuel pins plus two burnable poison pins with either 2% or 2.5% ^{10}B content. Each annular fuel pin (with an inner radius of 0.5 cm, an outer radius of 1.3 cm, a height of 54.6 cm, and a pitch between pins of 5.15 cm) is made of 14 fuel compacts, each 3.9 cm in height. The UO_2 fuel pins are enclosed in a graphite sleeve outside of which helium is circulated. The annular fuel pin contains on average 12,987 TRISO fuel particles embedded in a graphite matrix for a total mass of 188.58 ± 5.66 g of uranium. The TRISO grain is made of a relatively large spherical 0.03-cm-radius fuel kernel surrounded by four layers of carbon or silicon carbide. All of the material data used in the model were obtained from Reference [2].

2.2. Annular HTTR Critical Core Configurations

During the fuel loading in the HTTR core, several critical configurations were realized with the fuel distributed in different annular patterns and with the remaining full-core fuel column positions replaced by dummy graphite blocks. Cross-sectional views of annular critical cores are shown in Figure 2. To achieve criticality for these cores, the control rods were inserted at different depths, typically in a flat standard (FS) pattern (i.e., all inner control rods inserted to the same depths and the outer [ring 3] control rods fully withdrawn). The exceptions were the 19-fuel column configuration, in which the central pair of rods is primarily used to achieve criticality, and the 24-fuel column configuration, in which, besides an FS critical configuration, a second critical configuration was realized with an F23 pattern that uses the insertion of the control rods in rings 2 and 3.

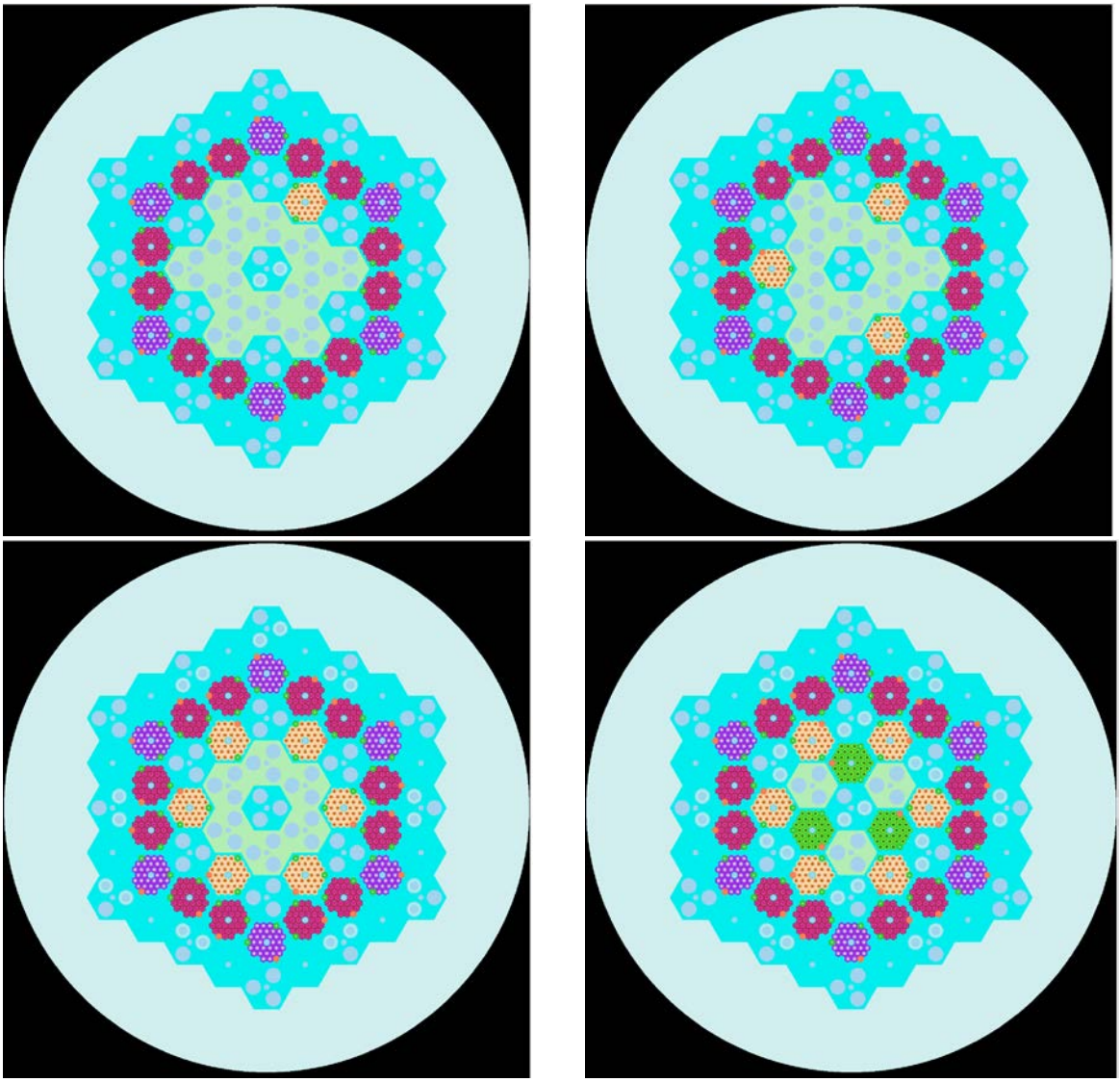

Figure 2. Partially loaded HTTR core configurations. From left to right and top to bottom: 19 fuel-column, 21 fuel-column, 24 fuel-column (F23 pattern), and 27 fuel-column.

3. SCALE CODES AND DATA

All ORNL simulations described in this paper were performed with SCALE6.1 (prerelease version) and used nuclear cross sections based on the ENDF/B-VII.0 data. The MCNP5 results used for comparisons in this paper were obtained with continuous energy (CE) cross sections based on ENDF/B-VII.0 nuclear data.

The material description used in the SCALE models is based on the latest revision of the experiment evaluation in the IRPhE handbook, revision 1, found in Reference [2]. Previously, results were obtained using revision 0 of this evaluation and were documented in Reference [5].

Two SCALE models were developed for the HTTR configurations, a CE model and a multigroup (MG) model. The difference between these two models consists not only in the use of a different cross-section library, CE versus MG, but also in the level of detail for geometric representation that must be consistent with the underlying assumptions for cross-section processing. In the SCALE CE model, the TRISO fuel particles in the fuel pin are explicitly represented using a cubic regular lattice placement. No effort was made to avoid particle clipping at the fuel pin boundaries. The same modeling approach was used for the MCNP models [2] that are used as a basis of comparison in this paper. As shown in Reference [2], the effect of using such a modeling assumption, which inherently leads to some particle clipping at the fuel pin boundary, has minimal consequences for the HTTR core eigenvalue calculations.

The SCALE MG model does not explicitly represent the fuel particles inside the fuel pin but uses a homogeneous mixture instead. However, it does account for the double-heterogeneity of the fuel through the way the cross-section self-shielding is carried out—using the double-heterogeneous (or DOUBLEHET) option for cross-section processing. The MG model required additional approximations and corresponding modeling effort to use the double-heterogeneous treatment for the annular fuel pins characteristic of HTTR. The double-heterogeneous treatment in SCALE only models solid cylindrical fuel pins, not annular pins. The fuel pin transformation that was chosen consisted in homogenizing the helium regions into the fuel pin matrix. This approximation was used both for applying the double-heterogeneous treatment to the cross-section processing and for the transport geometry model. The SCALE MG model used the 238-group cross-section library.

4. SIMULATION RESULTS

4.1. Criticality Simulations

The calculated multiplication factor (k) values for the critical configurations described in Section 2 are presented in Table I. This table shows the k values obtained with both the CE and the MG SCALE models, as well as the corresponding values calculated with MCNP reported in References [2] and [3].

Table I. Comparison of calculated and experimental multiplication factor for the six HTTR critical core configurations

Critical Configuration	Experimental		MCNP5	SCALE6.1 CE	SCALE6.1 MG
	k_{eff}[a]	Uncertainty[b]			
1. 19 columns	1.00490	0.01015	1.02760 (10)[c]	1.01702 (10)	1.01473 (8)
2. 21 columns	1.00370	0.00960	1.02970 (10)	1.02297 (9)	1.02104 (8)
3. 24 columns, FS	1.00370	0.00810	1.02490 (10)	1.01900 (9)	1.01649 (9)
4. 24 columns, F23	1.00370	0.00770	1.02870 (10)	1.01891 (9)	1.01629 (8)
5. 27 columns	1.00370	0.00715	1.02180 (10)	1.01491 (9)	1.01247 (8)
6. 30 columns (fully loaded)	1.00250	0.00650	1.02290 (10)	1.01633 (10)	1.01325 (8)

[a] The bias due to the removal of reactor instrumentation in the instrumentation columns is included [2, 3].
[b] Experimental uncertainties are averages of upper and lower uncertainty bounds as estimated in References [2] and [3].
[c] For this table and other tables in this paper, the numbers in parentheses are statistical standard deviations affecting the last digit(s) of the result. For example, 1.01702 (10) should be read as 1.01702 ± 0.00010.

The difference in the multiplication factor, $\Delta k = 10^5 \times \left(k_{code} - k_{\exp}\right)$, between different calculations and the experimental values, is graphically represented in Figure 3 for the six critical configurations. The error bars represent the sum of experimental uncertainty (dominant) and the statistical standard deviation (typically much smaller) added as for independent random variables. The average biases for the three simulations - SCALE6.1 MG, SCALE6.1 CE, and MCNP5 are 1201, 1449, and 2223 pcm, respectively, with a statistical standard deviation of ~300 pcm. The causes of these biases can range from insufficiently detailed description (geometry, materials, etc.) of the critical states to the quality of nuclear data used in simulations. For the MG model, additional approximations are needed for the cross sections used, some of them dependent upon the evaluator's subjectivity. The similarity of the deviations of the calculated multiplication factors from experiment for all three codes suggests that systematic modeling issues affect all three types of calculations.

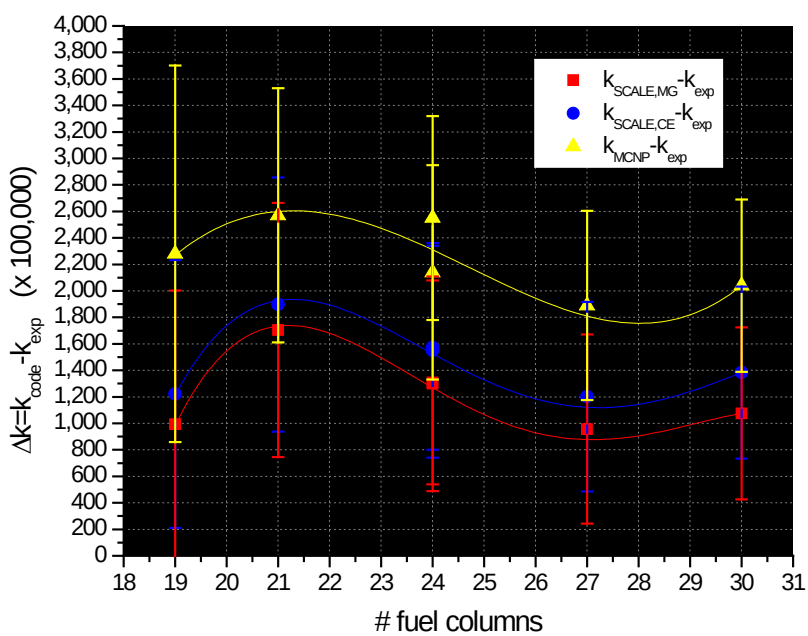

Figure 3. Difference in multiplication factors between simulations and experiment.

4.2. Simulation of Subcritical Full Core Configuration

Several subcritical configurations were also realized during the approach to criticality. Their descriptions, however, lack important elements for a correct simulation. Therefore, the only subcritical configuration modeled in this study is the full core (30-fuel-column) configuration with all control rods fully inserted (i.e., control rod tips are 55 mm below the bottom of the fuel). Table II summarizes the experimental and calculated multiplication factors for this configuration. The MCNP result is taken from Reference [2]. The experimental value is corrected for the bias introduced by the control instrumentation, as described in Reference [2]. There is better calculation–experiment agreement for this subcritical configuration—less than ~1200 pcm for both MCNP and SCALE—than that observed for the critical configurations. The experiment–calculation difference is close to the reported experimental uncertainty of 1000 pcm.

Table II. Multiplication constants for full core subcritical configuration

Subcritical Configuration	Experimental[a]	MCNP5	SCALE6.1 CE	SCALE6.1 MG
30 columns, all control rods fully inserted	0.68760 (1000)	0.69990 (10)	0.69899 (9)	0.69644 (8)

[a] For the experimental result, the number in parenthesis represents the uncertainty as evaluated in the HTTR criticality benchmark [2]. All of the other numbers in parentheses are statistical standard deviations.

4.3. Excess Reactivity

The excess reactivity can be calculated simply as

$$\rho = 100 \times \left(\frac{1}{k_{crit}} - \frac{1}{k_{CRup}} \right), \tag{1}$$

where k_{crit} is the multiplication constant corresponding to the critical configuration, and k_{CRup} is the multiplication constant corresponding to the reactor state with all control rods fully withdrawn. A reactor in a critical state should have $k_{crit} = 1$. For simulations, however, because of code biases and simulation uncertainties, $k_{crit} \neq 1$ and therefore the above relationship to calculate the excess reactivity cannot usually be simplified by setting $k_{crit} = 1$.

Taking into account the above arguments, the excess reactivity was calculated for each critical configuration by considering reactor states with the control rods fully withdrawn and with the control rods inserted so that a critical configuration is achieved. “Critical configuration” in this context means the core configuration with the control rods inserted as in the corresponding experimental critical configuration, although the multiplication factor produced by the calculation for such a configuration was not 1.0. The results of these simulations are listed in Table III. The statistical uncertainties for calculations, not included in the table, are typically below 0.01 %Δk/k for the SCALE calculations and below 0.02 %Δk/k for the MCNP

calculations. The experimental uncertainties [2] shown in Table III, typically 25–30%, are much larger than the statistical uncertainty of the corresponding calculated data.

Some ambiguity exists in the literature for the excess reactivity corresponding to the 19-column configuration. This excess reactivity is listed as 1.5 %Δk/k in Reference [6], but Reference [2] gives a value of 2.4 %Δk/k. The reason given in Reference [2] for this value is that this reactivity represents "the cumulative worth of fuel addition from the subcritical 18-fuel-column core and the 19-fuel-column core." This definition, however, would contradict the definition of excess reactivity given above in Eq. (1). A value of 1.5 %Δk/k was used for the calculations in the current paper. Also, the uncertainty of 0.24 %Δk/k associated with the excess reactivity for the 19 columns configuration simply represents 10% of the excess reactivity listed in Reference [2]. A well-documented basis for associating this uncertainty is not available in the literature. Given the uncertainties in the other values for the excess reactivities, it is reasonable to assume that this uncertainty is underestimated.

Table III. Excess reactivities for different fuel loadings

Core Fuel Loading	Experimental[a] (%Δk/k)	SCALE6.1 MG		SCALE6.1 CE		MCNP5	
		(%Δk/k)	(C-E)/E%[b]	(%Δk/k)	(C-E)/E%	(%Δk/k)	(C-E)/E%
18 columns	-0.9 ± 0.6	0.41[c]	-	0.39[c]	-	-	-
19 columns	1.5 ± 0.24	2.17	44.82	2.11	40.54	1.98	32.00
21 columns	4.0 ± 1.1	4.35	8.76	4.32	7.97	4.28	7.05
24 columns (FS)	7.7 ± 2.1	8.10	5.24	8.05	4.60	8.29	7.63
27 columns	10.7 ± 3.0	10.91	1.98	10.89	1.75	11.52	7.67
30 columns	12.0 ± 3.3	11.54	-3.82	11.49	-4.27	11.38	-11.79

[a] Experimental values are consistent with Reference [6].
[b] C is the calculated value and E is the experimental value, hence (C-E)/E is the relative departure of the calculation from experiment.
[c] See text for the procedure used to calculate this value.

Further ambiguity exists in the literature for the excess reactivity value of the (subcritical) 18-column configuration. Reference [7] gives a value of -0.3 %Δk/k for this reactivity. The value -0.9 %Δk/k listed as experimental in Table III, however, is taken from Reference [6] and is in agreement with the multiplication factor given in Reference [2] for an 18-column configuration.

Because the excess reactivity for the 18-column core is, in fact, a reactivity deficit (the configuration is subcritical) a particular approach was used in this paper to calculate the reactivity for this case. The SCALE-calculated data shown in Table III correspond to this approach. First, the multiplication factor for the configuration with all the control rods fully withdrawn (as one would calculate for the excess reactivity) was calculated. Then, this multiplication constant was corrected with the bias inferred from the 19-column critical core (Table I). The basis for this correction is that the multiplication factor listed in Table I corresponds to a critical configuration; hence, the true k_{eff} value should be 1.0. Finally, the reactivity was calculated using the expression shown in Eq. (1):

$$\rho = 100 \times \left(1 - \frac{1}{k_{CRup}^{18,corrected}} \right) = 100 \times \left(1 - \frac{1}{k_{CRup}^{18} - (k_{crit}^{19} - 1)} \right), \tag{2}$$

where k_{CRup}^{18} is the uncorrected value for the multiplication factor for the 18-column core configuration (all control rods fully withdrawn), and k_{crit}^{19} is the multiplication factor for the 19-column critical core as listed in Table I. The quantity $\left(k_{crit}^{19} - 1\right)$ represents the code bias (for the 19-column configuration, which was extended for correcting the 18-column core multiplication factor). The positive excess reactivity predicted for the 18-column core would indicate that the core can reach criticality with only 18 fuel columns, which does not correspond to experimental reality. The disagreement between the reported experimental data and the calculated result for this particular configuration may be due to uncertainty in code, data, or simplifying assumptions. For example, the correction described above for the bias is an *a posteriori* correction (it makes use of the knowledge of the criticality achieved with 19 fuel columns), and therefore the value such calculated for the excess reactivity for the 18-column configuration cannot be used to *a priori* predict the first criticality of the HTTR system. Note that applying the reported experimental uncertainty of 0.6 %Δk/k to the calculated result of 0.41%Δk/k to estimate the relevant ±1σ range would lead to positive, as well as negative, values for the excess reactivity. For comparison, Reference [5] calculates a reactivity of +0.8 %Δk/k for the 18-column configuration. The significance of the experiment–calculation comparison for this particular configuration indicated difficulty in predicting small excess reactivities that are close to zero.

Departure of the calculated values in Table III from the experiment shows a decreasing trend with an increase in the number of fuel columns. The quantity (C-E)/E% becomes negative (the computations underestimate the experimental value) when going from the partial cores to the full core loadings. As shown in Table III, there is an excellent agreement between the MG and CE SCALE results for all cases.

The experimental procedure for measuring excess reactivity, as described in Reference [2], assumed that a summation method from one critical state to the next was valid. Experimentally, after each fuel addition (e.g., from 21 fuel columns to 24 fuel columns), the control rods were inserted deeper into the core to maintain criticality. The additional depth to which the control rods were inserted gave the additional reactivity excess that was added by the increase in the amount of fuel. According to References [2] and [6], the reactivity was measured after each fuel addition using the inverse kinetics method. Neither of the above references describes this method. According to Reference [6], the excess reactivity was calculated with:

$$\rho_{ex} = \sum_i \Delta\rho_i^m R_i \ , \tag{3}$$

where $\Delta\rho_i^m$ is the increment in reactivity measured with the inverse kinetics method, and R_i is a correction factor inferred through calculation

$$R_i = \frac{\Delta\rho_i^v}{\Delta\rho_i^a} \ , \tag{4}$$

where $\Delta\rho_i^v$ is the increment in reactivity calculated with all the control rods fully withdrawn, and $\Delta\rho_i^a$ is the increment in reactivity for the actual control rod pattern for configuration *i*.

The evaluation procedure for the excess reactivity discussed above indicates that the numbers presented as experimental data are not based purely on experimental measurements, but also use corrections based on calculations (diffusion calculations in this case). These corrections are necessary to account for the shadowing effect of the control rods.

The incremental change in the excess reactivity (i.e., the quantity $\Delta\rho_i^m R_i$ for *i*=24, 27, and 30 fuel columns) was also evaluated for this paper by considering the reactivity added through fuel addition. The results are presented in Table IV.

Table IV. Incremental excess reactivities for different fuel loadings

Core Fuel Loading	Experimental (%Δk/k)	SCALE MG		SCALE CE		MCNP	
		(%Δk/k)	(C-E)/E%	(%Δk/k)	(C-E)/E%	(%Δk/k)	(C-E)/E%
24 columns (FS)	3.7 ± 1.0	3.69	-0.3	3.72	0.5	4.01	8.27
27 columns	3.0 ± 0.9	3.04	1.4	3.06	1.9	3.23	7.76
30 columns	1.3 ± 0.3	1.50	15.5	1.53	19.6	1.30	0.08

As shown in Table IV, the agreement between SCALE calculations and experiment is very good for 24 and 27 columns, but the difference is larger for the fully loaded core. The opposite is true for the MCNP estimations (from Reference [2]). All of the calculations, however, are within the uncertainties of the experimental evaluations.

4.4. Shutdown Margin

For the purpose of this analysis, and to be consistent with the reported measurement data, the "shutdown margin" definition differs from the one used by the U.S. Nuclear Regulatory Commission (NRC). In NRC's glossary of terms, "shutdown margin" is defined as: "the instantaneous amount of reactivity by which the reactor is subcritical or would be subcritical from its present condition assuming all full-length rod cluster assemblies (shutdown and control) are fully inserted except for the single rod cluster assembly of highest reactivity worth that is assumed to be fully withdrawn."

The shutdown margin, as used in this section and as measured experimentally, was evaluated for two cases of the fully loaded core configuration:

1. The first case (reflector control rods (CR) in) assumes that the central and first ring of control rods (C and R1 rods in Figure 1) maintain their position at critical configuration, while the reflector rods (R2 and R3) are fully inserted 55 mm below the bottom of the fuel blocks.
2. The second case corresponds to full insertion of all control rods.

The reactivity insertion was calculated using the following relationship:

$$\rho = 100 \times \left(\frac{1}{k_{CRin}} - \frac{1}{k_{crit}} \right), \tag{5}$$

where k_{crit} is the multiplication constant corresponding to the critical configuration and k_{CRin} is the multiplication constant corresponding to any of the two shutdown configurations with control rods inserted.

As mentioned above, for a critical system, we should have $k_{crit} \equiv 1$, but because of code biases and approximations in the computational models, the computed value can be different from 1. The results of the two simulations are listed in Table V for both the CE and MG SCALE models. Also listed are the experimental results with the assessed uncertainties as well as the MCNP simulation results (from Reference [2]).

Table V. Shutdown reactivities for full core configuration

Configuration	Experimental (% Δk/k)	SCALE6.1 MG (% Δk/k)	SCALE6.1 CE (% Δk/k)	MCNP5 (% Δk/k)
Reflector CR in	-12.1 ± 0.6	-9.13	-9.06	-9.27
All CR in	-46.3 ± 1.2	-45.29	-45.16	-46.59

Agreement of the SCALE results with the experiment is within the estimated experimental uncertainty for the case with all control rods inserted. A difference of ~25% between experimental and calculated data is observed for both SCALE and MCNP models for the case in which only the radial reflector control rods are inserted. Because the computational results are consistent and show the same departure from the experiment, it may be possible that this large difference is due to an uncertainty in the data used in these models, such as the position of the control rods.

The computational results shown in Table V are consistent with those published in Reference [6], in which a diffusion code was used: -8.6% Δk/k and -42.9% Δk/k shutdown margin for the two cases, respectively.

4.5. Control Rod Worths

The worth of each control rod is an important parameter in reactor operation. Knowing the differential worth of each control rod and/or bank of control rods (calibration curve) allows for correct gauging of different reactivity effects. During normal operation, the core is assumed to be critical at all times. The reactivity insertion from different mechanisms, such as fuel addition, temperature increase, xenon buildup, fuel depletion, etc. is compensated for by the movement of the control rods in such a way that the reactor is kept critical. Therefore, measuring the insertion depth of the control rods allows estimation of the reactivity effects produced by different events, if the worth of the control rods is known as a function of their depth.

The recent literature on HTTR experiments (References [2], [4] and [6]) mentions two types of control rod worth measurements. The first measurement is for the worth of a control rod at the center of the HTTR core. The description of this measurement, however, lacks important elements, and an attempt in Reference [2] to reproduce the experimental data was unsuccessful. The set of data for the second experiment is described in Reference [4] in the context of its use for estimating the temperature reactivity coefficients and is presented as a calibration curve (reactivity as a function of the control rod position) for an FS pattern in the fully loaded core. The specification of the FS pattern is sufficient to fully characterize the core configuration.

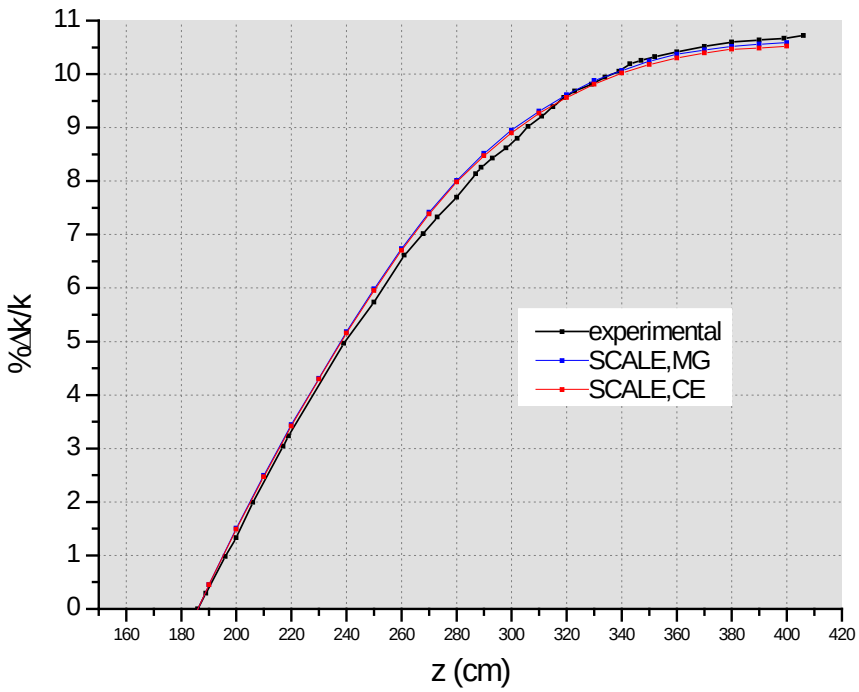

Figure 4. Control rod worth for the FS pattern.

Given the above considerations, only the second control rod worth measurement was used for this SCALE validation study. The reference results were obtained by digitization of the experimental curve in Figure 2.8 of Reference [4]. The control rod reactivity worth was evaluated by varying the position of the control rods in the fully loaded core. All control rods, except those in ring R3 (see Figure 1) that were fully withdrawn, were synchronously moved in an FS pattern. For each control rod height, the multiplication constant was calculated. As in Figure 2.8 of Reference [4], the reference position for a control rod insertion height was considered to be ~186 cm. The quantity calculated was

$$\%\frac{\Delta k}{k} \equiv 100 \times \left(\frac{1}{k_{ref}} - \frac{1}{k_h} \right), \qquad (6)$$

where k_{ref} is the multiplication constant corresponding to the reference insertion (~186 cm) of the control rods, and k_h is the multiplication constant corresponding to insertion height h.

Figure 4 presents the digitized experimental curve from Reference [4] together with the MG and CE SCALE6.1 calculated data. Agreement between experiment and calculation is very good over the whole range of the measurements. A slight overprediction of the control rod worth can be seen in the middle range of the curve (corresponding to the control rod tip near the top of the fuel) and an underprediction in the high range (corresponding to the control rod tip in the top axial graphite [i.e., the control rod fully extracted]). Agreement between the MG and CE SCALE models is very good.

4.6. Isothermal Reactivity Coefficients

4.6.1. Numerical calculation of reactivity coefficients

The isothermal temperature coefficient of reactivity can be obtained in an elegant way by considering the definition of the reactivity insertion $\Delta\rho$ when the temperature is raised from a temperature T_1 to a temperature T:

$$\Delta\rho(T,T_1)=\left(1-\frac{1}{k(T)}\right)-\left(1-\frac{1}{k(T_1)}\right)=\left(\frac{1}{k(T_1)}-\frac{1}{k(T)}\right). \tag{7}$$

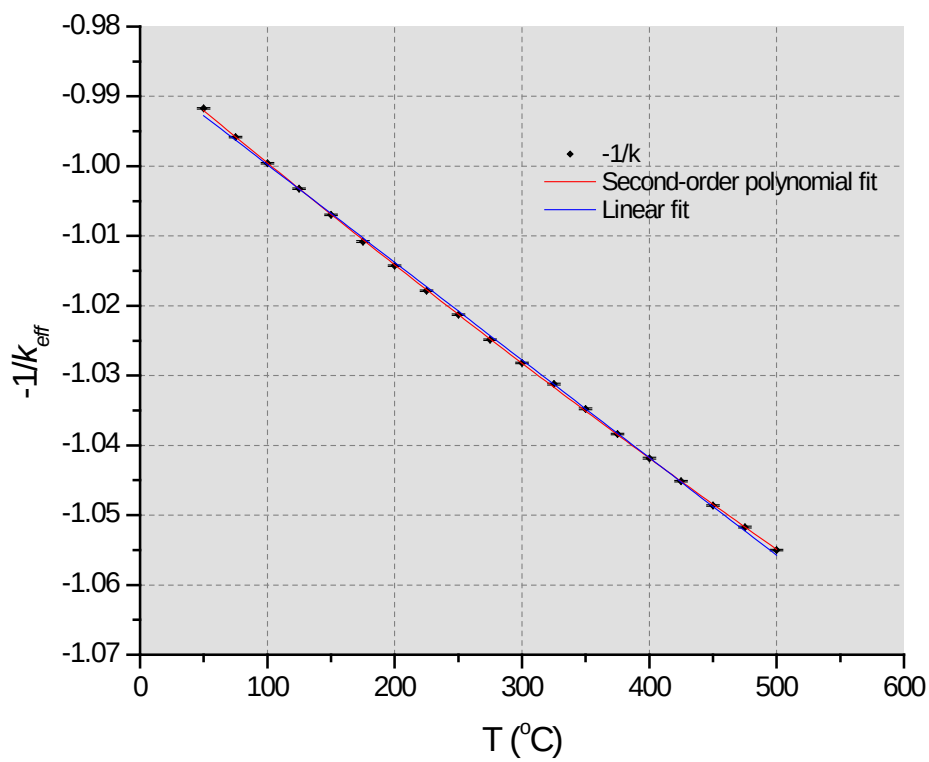

Figure 5. Polynomial fittings of the calculated multiplication factor dependence on temperature.

The average isothermal temperature coefficient of reactivity $\alpha(T,T_1)$ between temperatures T_1 and T will then be

$$\alpha(T,T_1) \equiv \frac{\Delta\rho(T,T_1)}{T-T_1} = \frac{1}{T-T_1}\left(\frac{1}{k(T_1)} - \frac{1}{k(T)}\right) = -\frac{\frac{1}{k(T_1)} - \frac{1}{k(T)}}{T_1 - T}. \quad (8)$$

An isothermal temperature coefficient of reactivity $\alpha(T)$ at temperature T can then be defined as

$$\alpha(T) \equiv -\lim_{T_1 \to T} \frac{\frac{1}{k(T_1)} - \frac{1}{k(T)}}{T_1 - T} = -\frac{\partial}{\partial T}\left(\frac{1}{k(T)}\right). \quad (9)$$

Equation (9) indicates that the isothermal temperature coefficient of reactivity can be calculated from the derivative of the curve $\frac{1}{k} = f(T)$. This is especially useful when a simple analytical fitting curve can be used for the representation of the dependence of $\frac{1}{k}$ on temperature. Figure 5 shows an example of the use of this method for the calculation of the isothermal reactivity coefficient for HTTR.

The procedure described above for the isothermal temperature coefficient of reactivity can be extended to the calculation of any other reactivity coefficient or to the calculation of control rod worth sensitivities with respect to the control rod insertion depth.

4.6.2. Isothermal reactivity coefficient for HTTR

The isothermal temperature coefficient of reactivity was calculated for the HTTR full core MG model with control rods inserted as in the cold critical configuration for a temperature range up to 500°C. From the linear fit in Figure 5, the average isothermal reactivity coefficient for HTTR over the temperature interval [50,500]°C can be calculated as

$$\overline{\alpha} = -(14.0 \pm 0.1) \text{ pcm/°C}. \quad (10)$$

A better approximation can be obtained with a second-order polynomial fit for the computed points on Figure 5, which leads to a linear dependence on temperature for the reactivity coefficient:

$$\alpha(T) = -(15.3688 \pm 0.1416) + (0.00253 \pm 0.00026)T[°C] \text{ pcm/°C}. \quad (11)$$

Table VI and the plot in Figure 6 compare the experimental values for different temperatures, the MCNP calculated values as reported in Reference [4], and the SCALE6.1 MG results. For the MG SCALE model, the cross-sections can be interpolated between the values corresponding to two different temperatures in the library to generate problem-dependent cross sections corresponding to the desired material temperature. This is an automated process and needs no intervention from the user. For both MCNP and SCALE CE, it is not possible to interpolate the SCALE CE cross-section data vs. temperature. The SCALE results were obtained for a fixed insertion depth of the control rods corresponding to the critical configuration.

As observed in Figure 6, the experimental errors were large, and the calculated values fall within the experimental uncertainty range or are marginally outside for all of the points, for both MCNP and SCALE.

Table VI. Isothermal reactivity coefficients

T(°C)	∂ρ/∂T (pcm/°C) Experimental	∂ρ/∂T (pcm/°C) MCNP	∂ρ/∂T (pcm/°C) SCALE6.1 MG
72.85	-12.3 (3.2)	-11.6 (0.2)	-15.0 (0.1)
133.85	-13.2 (3.3)	-12.8 (0.2)	-14.7 (0.1)
147.85	-21.7 (13)	-12.8 (0.2)	-14.6 (0.1)
259.85	-16.5 (2.9)	-12.9 (0.2)	-14.1 (0.2)
368.85	-10.3 (2.8)	-12.6 (0.2)	-13.5 (0.2)
462.85	-8.6 (2.7)	-12.1 (0.2)	-13.0 (0.2)

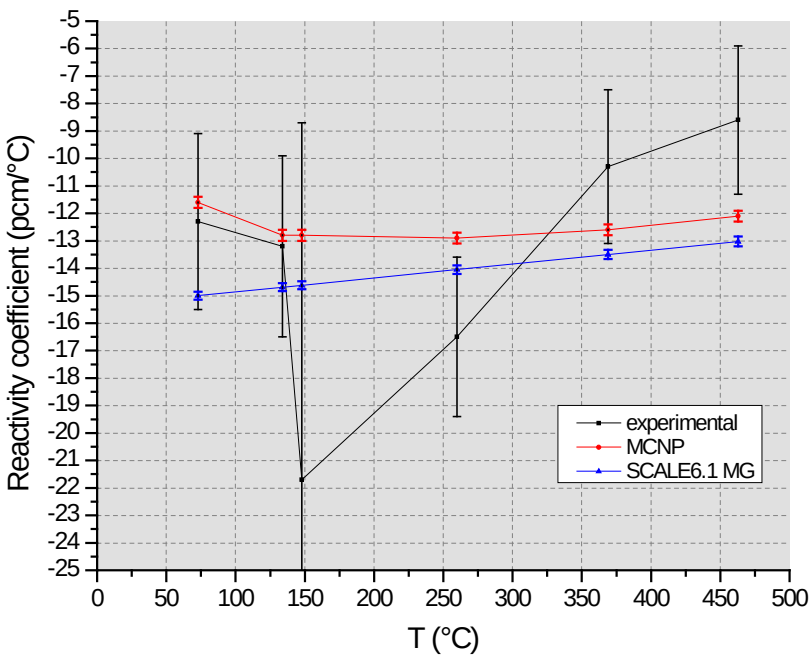

Figure 6. Isothermal reactivity coefficients for HTTR.

4.7. Flux and Reaction Rate Distributions

4.7.1. Distributions for the fully loaded core

The neutron flux and ^{235}U fission reaction rates were calculated along one of the irradiation columns of the 30-fuel-column (full) HTTR core (see Figure 1). The experiment measured the fission rate using a fission chamber at selected heights along the irradiation column, and the reported value was normalized to the largest value [2].

Comparison of the SCALE-computed scalar fluxes and the experimental fission rate values is shown in Figure 7. The agreement is reasonable, similar to the agreement between MCNP computations and experiment, as reported in Reference [2]. It is interesting to note that if the experimental values were reported at fission chamber height values shifted by 10 cm (to the right on Figure 7), the agreement between experiment and calculations would be almost perfect. Agreement between the values calculated with the MG and CE SCALE models is very good. The flux distributions calculated along the other two irradiation channels were almost identical to the one shown in Figure 7 and therefore not plotted. The computed reaction rates shown in the figure were obtained using the ^{235}U(n,f) cross sections on the ENDF/B-VII.0 library (infinite dilution cross section). A more rigorous calculation would have to take into account the structure and the self-shielding of the fission chamber . It is evident that the use of the fission reaction rate instead of the flux for the computed values brings the calculations slightly closer to the experiment. The statistical standard deviations for the computed values are very small and were omitted from the figure for clarity.

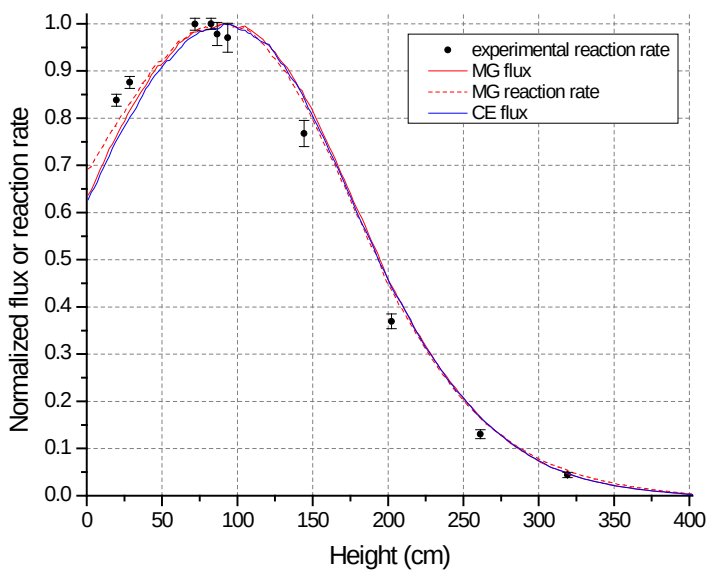

Figure 7. Flux and ^{235}U(n,f) reaction rate distributions along the irradiation channel for critical HTTR full core.

The closeness of the normalized scalar flux distribution and corresponding normalized reaction rate can be explained by looking at the definition of the latter:

$$\frac{\int_0^\infty n\sigma_f(\vec{r},E)\Phi(\vec{r},E)dE}{\int_0^\infty n\sigma_f(\vec{r}_0,E)\Phi(\vec{r}_0,E)dE}, \qquad (12)$$

where n is the number density of the ^{235}U, σ_f is the microscopic fission cross section, Φ is the neutron flux, and $\vec{r}_0$ is the position corresponding to the maximum value of this ratio. Because the macroscopic cross section is independent of position when the infinite dilution microscopic cross section is used, the above ratio is identical to the ratio of the scalar fluxes $\frac{\int_0^\infty \Phi(\vec{r},E)dE}{\int_0^\infty \Phi(\vec{r}_0,E)dE}$ (normalized fluxes) if, for example, the flux is a separable function of position and energy. The implication is that the spectrum of the neutrons reaching the fission chamber is almost independent of the position of the chamber in the irradiation column.

4.7.2. Flux and reaction rates distributions for the 24 fuel-column critical configuration with FS control rod pattern

The normalized flux and the calculated and experimental fission reaction rates for the 24-fuel-column critical configuration with control rods in an FS pattern, identified as configuration 3 in Table I, are illustrated in Figure 8. The level of agreement between calculations and experiment and the shape of the distributions are very similar to those obtained for the full core (30-column) configuration. The reason for the shape similarity is the similarity of the control rod patterns for the two configurations, although the insertion depth is different.

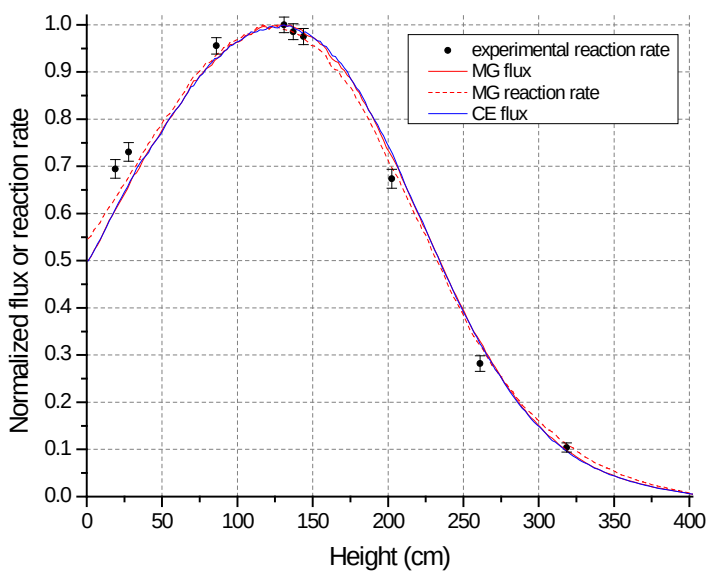

Figure 8. Flux and ^{235}U(n,f) reaction rate distributions along the irradiation channel for critical HTTR core configuration 3.

4.7.3. Flux and reaction rates distributions for the 24-fuel-column critical configuration with F23 control rod pattern

Configuration 4 is the 24-fuel column critical configuration with control rods in an F23 pattern. Because the control rods are inserted in a different pattern, the flux and reaction rate

distributions, illustrated in Figure 9, are different from those corresponding to the 24-column core with an FS control rod pattern. The most interesting point about the distributions for configuration 4 is that using the reaction rate distribution instead of the flux makes an important difference; the calculated reaction rate distribution is in significantly closer agreement with the experimental reaction rates.

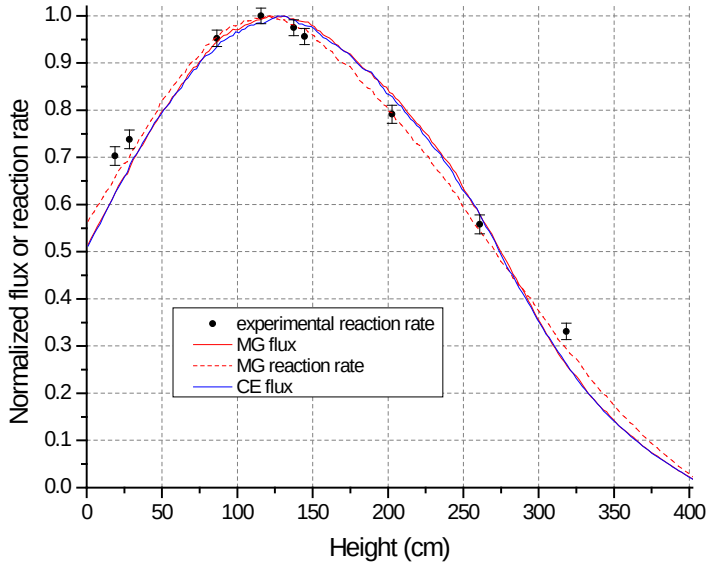

Figure 9. Flux and ^{235}U(n,f) reaction rate distributions along the irradiation channel for critical HTTR core configuration 4.

5. CONCLUSIONS

A thorough validation study was performed with the SCALE code system using experimental data for the fresh HTTR core configurations. Ample documentation exists in literature describing tests performed on this reactor. The SCALE simulations discussed in this paper relied primarily upon data published over the past 3 years by INL, which undertook the task of consolidating the available documentation in three IRPhE benchmarks. The SCALE results presented in this paper were obtained with models based on benchmark descriptions from the most recent IRPhE revisions [2]. Compared with calculated results [5] obtained based on earlier revisions of these benchmarks, the calculated multiplication factors are closer to the experimental values by ~200 to 300 pcm. The calculated differential quantities, however, do not change significantly with the benchmark specifications revision.

With rare exceptions (notably, the isothermal reactivity coefficient), all SCALE calculations were performed using both CE and MG (238-group) cross sections based on ENDF/B-VII.0 nuclear data. The CE SCALE model uses an explicit representation of the fuel grains similar to the one used in the MCNP simulations. The MG model uses the double-heterogeneity feature incorporated in SCALE to model homogenized solid (i.e., non-annular) cylindrical fuel pins.

Data at the core level were compared with available experimental data and with results obtained with MCNP, as documented in References [2], [3], and [4]. The simulation results generally show very good agreement with the experimental values. The multiplication factors also agree very well (typical differences of ~200 to 300 pcm) between the MG and CE SCALE models. The difference between results for the two models is slightly larger (~300-pcm) for the full core eigenvalue simulations but still within an acceptable range. Excellent agreement is observed for differential quantities (excess reactivity, shutdown margin, control rod worths) between the MG and CE models. Excellent agreement was also observed for the spatial neutron flux distributions.

Agreement of the calculated and experimental data is generally within acceptable limits for differential quantities. Comparison of the calculated k_{eff} values to experimental values indicates that a positive bias exists in the simulation model. This bias is common to both SCALE and MCNP models. The SCALE model bias is between 1.5 and 2% for the six critical configurations with the CE model and slightly lower (by ~0.2 to 0.3%) with the MG model. The bias in the MCNP model is higher (1.8 to 2.6%), probably due to differences in modeling and cross-section data. The causes of these biases can range from uncertainties in material data (boron content in particular) to insufficient geometric detail to the nuclear data used. Preliminary results obtained at ORNL indicate that increasing the absorption cross section in carbon, as in the recently released JENDL 4.0 library, can lead to a reduction of ~1% in the bias to below 1% with the SCALE models.

In conclusion, it was shown that the SCALE code system is capable of accurate simulations for the fresh HTTR core. These conclusions, though, cannot be extended to higher temperatures or to mid-cycle simulations without further confirmatory calculations.

ACKNOWLEDGMENTS

The work described in this paper was sponsored by the U.S. Nuclear Regulatory Commission Office of Research.

REFERENCES

1. *SCALE: A Comprehensive Modeling and Simulation Suite for Nuclear Safety Analysis and Design*, ORNL/TM-2005/39, Version 6.1, Oak Ridge National Laboratory, Oak Ridge, TN (2011). (Available from Radiation Safety Information Computational Center at Oak Ridge National Laboratory as CCC-785.)
2. J. D. Bess and N. Fujimoto, evaluators, “Evaluation of the Start-up Core Physics Tests at Japan’s High Temperature Engineering Test Reactor (Fully-Loaded-Core)”, HTTR-GCR-RESR-001, Revision 1, *International Handbook of Evaluated Reactor Physics Benchmark Experiments*, 2010.
3. J. D. Bess and N. Fujimoto, evaluators, “Evaluation of the Start-up Core Physics Tests at Japan’s High Temperature Engineering Test Reactor (Annular Core Loadings),” HTTR-GCR-RESR-002, Revision 0, *International Handbook of Evaluated Reactor Physics Benchmark Experiments*, 2010.
4. J. D. Bess and N. Fujimoto, evaluators, “Evaluation of Zero-Power, Elevated-Temperature Measurements at Japan’s High Temperature Engineering Test Reactor,” HTTR-GCR-RESR-

003, Revision 0, *International Handbook of Evaluated Reactor Physics Benchmark Experiments*, 2011.
5. G. Ilas, D. Ilas, R. P. Kelly, E. E. Sunny, *Validation of SCALE for High Temperature Gas-Cooled Reactor Analysis*, ORNL/TM-2011/161, Oak Ridge National Laboratory, Oak Ridge, TN, November 2011.
6. N. Nojiri, S. Shimakawa, N. Fujimoto, M. Goto, "Characteristic Test of Initial HTTR Core", *Nuclear Engineering and Design*, **233**, pp. 283-290 (2004).
7. S. Shimakawa, M. Goto, S. Nakagawa, Y. Tachibana,"Impact of Capture Cross-Section of Carbon on Nuclear Design for HTGRs", *Proceedings of HTR2010*, Prague, Czech Republic, October 18-20, 2010.